Title
Nitric Oxide Synthase as a Target for Methicillin-Resistant Staphylococcus aureus.

Journal
Chemistry & biology, 22(6)

ISSN
1074-5521

Authors
Holden, Jeffrey K
Kang, Soosung
Beasley, Federico C
et al.

Publication Date
2015-06-01

DOI
10.1016/j.chembiol.2015.05.013

HHS Public Access

Author manuscript

Chem Biol. Author manuscript; available in PMC 2016 June 18.

Published in final edited form as:

Chem Biol. 2015 June 18; 22(6): 785–792. doi:10.1016/j.chembiol.2015.05.013.

Nitric Oxide Synthase as a Target for Methicillin Resistant *Staphylococcus aureus*

Jeffrey K. Holden[a], **Soosung Kang**[b], **Federico C. Beasley**[c], **Maris A. Cinelli**[b], **Huiying Li**[a], **Saurabh G. Roy**[d], **Dillon Dejam**[a], **Aimee L. Edinger**[d], **Victor Nizet**[c], **Richard B. Silverman**[b,*], and **Thomas L. Poulos**[a,*]

[a]Departments of Molecular Biology and Biochemistry, Pharmaceutical Sciences, and Chemistry, University of California, Irvine, CA 92697-3900

[b]Departments of Chemistry and Molecular Biosciences, Chemistry of Life Processes Institute, Center for Molecular Innovation and Drug Discovery, Northwestern University, Evanston, IL 60208-3113

[c]Departments of Pediatrics and Skaggs School of Pharmacy and Pharmaceutical Sciences, University of California, San Diego, California 92093

[d]Department of Developmental and Cell Biology, University of California, Irvine, CA 92697

Summary

Bacterial infections associated with methicillin-resistant *Staphylococcus aureus* (MRSA) are a major economic burden to hospitals and confer high rates of morbidity and mortality amongst those infected. Exploitation of novel therapeutic targets is thus necessary to combat this dangerous pathogen. Here we report on the identification and characterization, including crystal structures, of two nitric oxide synthase (NOS) inhibitors that function as antimicrobials against MRSA. These data provide the first evidence that bacterial NOS (bNOS) inhibitors can work synergistically with oxidative stress to enhance MRSA killing. Crystal structures show that each inhibitor contacts an active site Ile residue in bNOS that is Val in the mammalian NOS isoforms. Mutagenesis studies show that the additional nonpolar contacts provided by the Ile in bNOS contributes to tighter binding of the bacterial enzyme.

Graphical abstract

*Corresponding Authors: Thomas L. Poulos poulos@uci.edu; Richard B. Silverman Agman@chem.northwestern.edu.

Accession codes

Coordinate and structure factor files were deposited in the Protein Data Bank with the following accession codes: 4D7H, 4D7I, 4D7J, and 4D7O

Author contributions JKH designed and carried out the crystallographic and enzyme assay experiments; SK and MAC did the chemical synthesis in the lab of RBS; HL assisted with X-ray data collection; DD assisted JKH with protein preparation; FCB carried out the MRSA experiments in the lab of VN; SGR evaluated NOS inhibitor cytotoxicity in the lab of ALE; JKH and TLP wrote the paper and VN and RBS edited the paper.

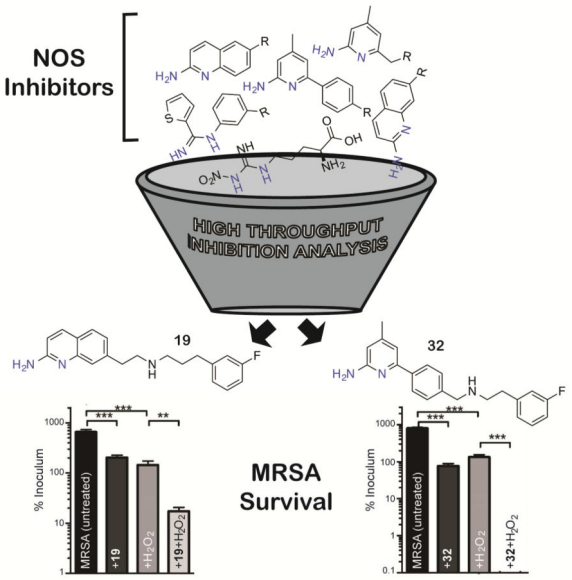

Introduction

As bacterial pathogens continually acquire resistance to commonly used antibiotics, it has become clear that novel therapeutic strategies are required to combat serious infections (Talbot et al., 2006). In particular, there is an urgent need for the development of new pharmaceuticals that target the preeminent Gram-positive human bacterial pathogen methicillin-resistant *Staphylococcus aureus* (MRSA). MRSA, a Gram-positive pathogen resistant to common β-lactam antibiotics (Loomba et al., 2010), was first reported in 1961(Jevons et al., 1961) and remains one of the most costly bacterial infections worldwide (Diekema et al., 2001). MRSA is a major threat to public health because of the high prevalence among nosocomial infections and the emergence of highly virulent community-associated strains and their varying epidemiology (Stefani et al., 2012). In recent years, the threat of MRSA has been heightened by reports of strains resistant to vancomycin, as this agent is often considered the drug of last resort (Gardete and Tomasz, 2014). Characterization and exploitation of alternative bacterial drug targets will be essential for future management of MRSA infections.

Recent gene deletion experiments in *S. aureus*, *Bacillus anthracis*, and *B. subtilis* have implicated bacterial nitric oxide synthase (bNOS) as a potential drug target, since this enzyme provides the bacterial cell a protective defense mechanism against oxidative stress and select antibiotics (Gusarov et al., 2009; Shatalin et al., 2008; van Sorge et al., 2013). In Gram-positive pathogens, it has been proposed that bacterial NO functions to remove damaging peroxide species by activating catalase and to limit damaging Fenton chemistry by nitrosylating thioredoxins involved in recycling the Fenton reaction (Gusarov and Nudler, 2005; Shatalin et al., 2008). We recently provided an initial proof of principle regarding pharmacological targeting of bNOS, as growth of the nonpathogenic model organism *B. subtilis* was severely perturbed in response to combination therapy with an active site NOS inhibitor and an established antimicrobial (Holden et al., 2013).

Design and development of a potent bNOS inhibitor against bone fide pathogens such as MRSA is complicated by the active site structural homology shared with the three mammalian NOS (mNOS) isoforms (Pant et al., 2002): neuronal NOS (nNOS), inducible NOS (iNOS), and endothelial NOS (eNOS). It is especially important not to inhibit eNOS given the critical role eNOS plays in maintaining vascular tone and blood-pressure (Yamamoto et al., 2001). Selectivity over nNOS may represent less of an immediate problem, since many of the polar NOS inhibitors characterized thus far are not very effective at crossing the blood-brain barrier (Silverman, 2009). Recent structure-based studies utilizing *B. subtilis* NOS (bsNOS) as a model system for bNOS suggest that specificity can be achieved through targeting the pterin-binding site (Holden et al., 2013; Holden et al., 2014), as the bNOS and mNOS pterin binding sites are quite different.

To quickly identify potent bNOS inhibitors we screened a diverse set of NOS inhibitors (Figure 1) using a novel chimeric enzyme recently reported for bNOS activity analysis (Holden et al., 2014). From this high-throughput analysis we were able to identify two potent and chemically distinct bNOS inhibitors. Crystal structures and binding analyses of these inhibitors revealed both to bind a hydrophobic patch within the bNOS active site. Moreover, both compounds possess antimicrobial activity against *S. aureus*, suggesting that these NOS inhibitors could represent viable new drug leads against this foremost human pathogen so frequently resistant to current antimicrobials.

Results and Discussion

Identification of Potent bNOS Inhibitors

Rapid identification of molecular fragments that function as potent bNOS inhibitors is a key initial step toward the design and characterization of future bNOS inhibitors. To carry this out, we adapted a bNOS activity assay (Holden et al., 2014) to screen through a series of NOS inhibitors using a single time point approach (Fig 2). Concurrently, we measured the K_S for each inhibitor using the imidazole displacement assay. In both of these studies bsNOS was utilized as a model system, since bsNOS assays are well developed and bsNOS shares high active site sequence homology with *S. aureus* and *B. anthracis* NOS enzymes. While all inhibitors bound to bsNOS in the μM range, the most potent bsNOS inhibitors identified from the activity analysis were calculated to have K_S values in the low μM to nM range. Using the single time point approach in combination with the imidazole displacement assay, we identified compounds that were both potent inhibitors and tight binders to the active site. Since L-NNA is an excellent inhibitor analog of the NOS substrate L-Arg, the potency of L-NNA at 40.9 ± 5.3% nitrite (Fig 2) was established as an arbitrary threshold for identifying designer molecules with increased potency. Using L-NNA as a benchmark led us to classify several NOS inhibitors as potent bNOS inhibitors. This group includes three aminoquinoline inhibitors, two 6-benzyl aminopyridine inhibitors, and two aminopyridine inhibitors. Of the two aminopyridine inhibitors, **7** was previously described as a NOS inhibitor with antimicrobial properties (Holden et al., 2013). Since we previously characterized the binding of aminopyridine inhibitors to bsNOS, we selected the most potent aminoquinoline and 6-benzylaminopyridine based inhibitors, **19** and **32**, respectively, for further analysis. Compounds **19** and **32** were also the two most potent inhibitors of the 37

NOS inhibitors evaluated using the bsNOS single time point analysis at 6.1% nitrite and 13.2% nitrite, respectively. In addition, inhibitor potency of **19** and **32** was a direct result of competing with substrate at the active site, as neither compound influenced electron transfer rates or the Griess reaction chemistry used to measure bNOS activity (Fig S1 and Table S1).

Isoform Selectivity of NOS Inhibitors

Compounds **19** and **32** were next assayed separately against purified NOS isoforms at varying concentrations (Holden et al., 2014). Even though the IC_{50}s for both mNOS and bsNOS were measured by complimentary methods, both methods allowed for an excellent comparison of inhibitor potency, as IC_{50} was used to calculate K_i using the Cheng-Prusoff equation (Cheng and Prusoff, 1973). From our K_i analysis (Table 1), it is clear that both **19** (269 nM) and **32** (1940 nM) function as potent bNOS inhibitors and demonstrate excellent selectivity over both iNOS and eNOS (Table 1). Though selectivity over nNOS remains an issue it is unclear whether cross-reactivity with nNOS expressed in neuronal tissues would represent an important limiting factor for these drugs during short course antibacterial therapy unless blood-brain penetration was high; indeed, nNOS inhibition itself has been examined as a treatment for Parkinson's disease in a rat model (Yuste et al., 2012).

To better understand the structural basis for inhibitor potency and selectivity we solved inhibitor bound crystal structures of **19** and **32** (Fig 3, Table 2). Both **19** and **32** were co-crystallized in the presence of the pterin molecule H_4B. However, the physiological pterin group for bNOS remains unclear as many bNOS containing bacteria do not contain the biosynthetic machinery required for H_4B synthesis (Pant et al., 2002). Previous work showed the ubiquitous pterin, tetrahydrofolate, supports NO production by bNOS (Adak et al., 2002; Reece et al., 2009). In NOS crystal structures, H_4B binding is stabilized by a H-bond to heme propionate D, a H-bond with a conserved Arg residue, and a π-π stacking interaction with a conserved Trp residue (Fig 3). The function of pterins in bNOS is unclear, although spectroscopic studies indicate pterins are not required for stability, as in mNOS; pterins are required for electron transfer in all NOS isoforms (Chartier and Couture, 2004).

Although **19** and **32** are chemically quite different, they both bind to the active site Glu-243 through a series of H-bonds, and do not interact with H_4B. For the nNOS inhibitor-bound crystal structures, the fluorinated-benzyl group of both **19** and **32** bound to a hydrophobic pocket adjacent to the heme propionate group. This hydrophobic pocket is composed of residues Leu-337 and Met-336 from the N-terminal Zn^{2+} binding motif and Tyr-706 (Figure 3A and 3B). Unlike nNOS, bNOS does not contain an N-terminal Zn^{2+} binding motif, and therefore does not contain an analogous hydrophobic pocket adjacent to the heme propionate. Despite slight differences in binding of the fluorinated-benzyl group, in both NOS isoforms binding of **19** and **32** was further stabilized by H-bonds between the secondary amine of each inhibitor and the heme propionate groups (Figures 3D and 3E). Direct comparison of the bsNOS-**19** and the previously reported nNOS-**19** (Cinelli et al., 2014) structures revealed the binding mode of **19** to be unchanged between the two NOS isoforms. However, the binding mode in bsNOS was further stabilized by the hydrophobic contact between Ile-218 and the aminoquinoline group of **19**. Since Ile-218 is within van der Waals contact of **19** and the analogous residue in nNOS is Val-567, our data suggest that the

slight differences in hydrophobicity between Ile and Val allow for improved binding of **19** to bsNOS.

Similar to **19**, crystal structure analysis of **32** demonstrates the inhibitor-binding mode to be further stabilized by the hydrophobic contact between the inhibitor and Ile-218 (Fig 3C and Fig S1). In both the nNOS-**32** and I218V-bsNOS-**32** crystal structures (Figs 3E and 3F, respectively), the inhibitor-binding mode of **32** is unchanged by the Ile/Val difference, as compared to WT bsNOS. To evaluate the contribution of Ile-218 to the inhibitor-binding mode we measured inhibitor binding using the imidazole displacement assay. From this analysis we found the inhibitor binding of both **19** and **32** to be ~5–6 fold tighter to Ile-218 over I218V (Table 3). Between the crystal structures and binding assay results, our data suggest that the increased hydrophobicity of Ile-218 over the analogous mNOS Val residue improves inhibitor binding to bNOS. This is partly observed in the crystal structures, as binding of **19** or **32** induces an alternative rotameric position in Ile-218 to form a hydrophobic contact with both **19** and **32** (Fig S1). Considering that Ile-218 is conserved across all bNOS enzymes (Wang et al., 2004), future inhibitors designed to target bNOS should continue to exploit Ile-218 by using the scaffolds of **19** and **32**.

Anti-MRSA Activity of NOS inhibitors

To evaluate the antibacterial potential of NOS inhibitors **19** and **32** on bacterial growth, we utilized the highly virulent CA-MRSA strain UAMS118 (*wt*) representative of the USA300 clonal lineage and a previously engineered isogenic NOS deletion mutant (van Sorge et al., 2013). Since previous experiments have shown bacterial Δ*nos* strains are more susceptible to H_2O_2-mediated killing (Holden et al., 2013; Shatalin et al., 2008; van Sorge et al., 2013), we measured the effect of NOS inhibitors and H_2O_2 on *S. aureus* (Fig 4). Our results both confirm that the Δ*nos* strain is more susceptible to H_2O_2-mediated killing compared to the *wt* strain and further demonstrate that co-treatment of *S. aureus* with H_2O_2 and a NOS inhibitor significantly increases the H_2O_2-mediated killing of the bacteria. Interestingly, both **19** and **32** exhibit some direct bacteria toxicity at 200 μM as demonstrated by the modest decrease in bacterial survival for both *wt* and Δ*nos* when treated with inhibitor alone (Fig 4). For example, **19** alone decreases growth by about 3-fold but with peroxide **19** decreases growth 30-fold. While this indicates a modest effect on non-NOS targets, the primary effect of **19** is to impart far greater sensitivity to oxidative stress and is consistent with **19** operating primarily by inhibiting bNOS. We also evaluated the toxicity of **19** and **32** using mouse embryonic fibroblast cells and found the IC_{50} values for **19** and **32** to be 5.84 μM and 11.86 μM (Table S2), respectively. These data indicate that toxicity of NOS inhibitors towards mammalian cells needs to be lowered for further consideration as a therapeutic agent.

The major effect of **19** and **32** is to work synergistically with H_2O_2 to significantly limit bacterial growth, most likely by limiting NO production. These results are consistent with previous results indicating that blocking of NO signaling increases bacterial susceptibility to oxidative stress(Gusarov and Nudler, 2005; Holden et al., 2013) and indicate **19** and **32** could perhaps function as antimicrobials to increase susceptibility to innate immune clearance via an oxidative burst. Furthermore, considering that many existing

pharmaceutical antibiotics function through an oxidative mechanism (Kohanski et al., 2007), bNOS inhibitors like **19** and **32** could theoretically synergize to increase the killing efficiency of such agents.

Significance

Nitric oxide (NO) generated by bacterial nitric oxide synthase (bNOS) helps to protect certain gram positive bacteria from oxidative stress including antibiotic-induced oxidative stress (Gusarov and Nudler, 2005; Gusarov et al., 2009; van Sorge et al., 2013). In earlier work, we found that a small number of inhibitors developed for selective nNOS inhibition also improved the efficacy of antimicrobials, suggesting that bNOS might be a viable drug target (Holden et al., 2013). In the present study we sought to achieve two goals. The first was to identify bNOS-selective inhibitors with antimicrobial activity against the important human pathogen, MRSA. Of the many compounds screened two were found to bind well to bNOS and exhibit antimicrobial activity with selectivity over eNOS and iNOS. Selectivity over eNOS is more important since interfering with eNOS will adversely effect the critical role that eNOS derived NO plays in maintaining vascular tone and blood pressure (Yamamoto et al., 2001). The second goal was to use crystallography to identify subtle differences between the bNOS and mNOS active sites to exploit for future inhibitor design. Ile-218 (Val in mNOS) contacts the inhibitors and that the I218V mutant exhibits about a 6-fold lower affinity than wild type. Although this is a rather modest difference, we have also found that several NOS inhibitors more readily bind to the pterin site in bNOS (Holden et al., 2015). Given the lower affinity of pterins for bNOS compared to mNOS, this is another important binding site difference between bNOS and mNOS. The Ile vs. Val active site difference together with the larger structural differences in the pterin site are critical molecular features that could be exploited in future inhibitor design efforts.

Experimental Procedures

Molecular Biology

Active site mutation I218V was introduced to *Bacillus subtilis* NOS (bsNOS) by site directed mutagenesis using PfuTrubo (Agilent). Both WT and I218V bsNOS were expressed and purified from *E. coli* as previously described for bsNOS (Pant et al., 2002). YumC and bBiDomain were also purified from *E. coli* and used for activity analysis (Holden et al., 2014). Recombinant rat nNOS and murine iNOS were expressed in *E. coli* and isolated as reported(Hevel et al., 1991; Roman et al., 1995).

Bacterial NOS Activity Inhibition

Reactions containing both bBiDomain (a chimera of bsNOS and redox partner YkuN) and YumC were initiated with NADPH and run for 4 min at 35 °C as previously described(Holden et al., 2014). Substrate N-omega-hydroxy-L-arginine (NOHA) and NOS inhibitor were included in each reaction at 200 μM and 30 μM, respectively. The Griess reaction was used to measure nitrite levels as a function of NOS activity. %Nitrite was calculated for each reaction as the concentration of nitrite detected in the presence of

inhibitor divided by the concentration of nitrite detected without inhibitor present. Each reaction was measured in duplicate for three separate trials.

K_i Determination

The K_i was calculated from the half maximal inhibitor concentration (IC_{50}) and K_D of L-NOHA using the Cheng-Prusoff equation (Cheng and Prusoff, 1973). For bBidomain the previously reported K_D of L-NOHA at 23.5 μM (Hannibal et al., 2011) was used to calculate K_i. IC_{50} was measured for bsNOS using bBiDomain and YumC as previously described (Holden et al., 2014). Cross reactivity of inhibitors **19** and **32** was checked over a concentration range of 0.01 to 50 μM inhibitor with the Griess reagents, and neither compound interfered or contributed towards the Griess reaction. IC_{50} for mammalian NOS was determined using the oxyhemoglobin assay as previously described (Huang et al., 2014).

Cytochrome-c oxidase Activity

Horse heart cytochrome C oxidase reduction was evaluated as previously described (Holden et al., 2014) using $\Delta\varepsilon_{550}$= 21 $mM^{-1}cm^{-1}$ (Martasek et al., 1999) and NADPH at 100 nM to initiate the reaction. For individual reactions containing a NOS inhibitor, inhibitor concentrations were set at 1 μM, 10 μM, and 50 μM inhibitor. Each reaction contained bBiDomain and YumC at 100 nM and 1 μM, respectively.

Crystallization and Structure Determination

Although the target of this study is *S. aureus*, we utilized bsNOS owing to the better diffraction power of bsNOS crystals. In fact, bsNOS and *S. aureus* NOS(Bird et al., 2002) are very similar and the crystal structures superimpose with a 0.55 Å root-meansquare-deviation of alpha carbon atoms. In addition, 32 of 33 residues within 10 Å of the heme iron and 14 of 17 residues within 10 Å of the pterin cofactor are identical. As a result structural insights gained from bsNOS are directly applicable to saNOS. Crystals of bsNOS and the I218V mutant were prepared using the hanging drop method by mixing protein at 18 mg/mL and well solution in a 1:1 ratio. Prior to crystallization the protein was stored in a buffer composed of 25 mM Bis-Tris methane at pH 7.4, 75 mM NaCl, 2% (vol/vol) glycerol, 0.5% (w/vol) PEG 3350, and 1 mM DTT. The well solution used for crystallization was composed of 60 mM Bis-Tris methane, 40 mM citric acid, 15% (w/vol) PEG3350, and 1.9% (vol/vol) 1-propanol at pH 7.6. Crystals grew overnight after seeding with old crystals. Crystals were cryoprotected in the well solution supplemented with 30% (vol/vol) glycerol, 2 mM H_4B, and 5–10 mM inhibitor prior to being flash frozen at 100 K. Crystals of rat nNOS oxygenase domain were prepared and flash frozen as previously described (Li et al., 2014). Data were collected under cryogenic conditions on individual crystals at both the Advanced Light Source (Berkeley, CA) and Stanford Synchrotron Radiation Lightsource (Menlo Park, CA). The raw data frames were indexed and integrated using either iMOSFLM (Battye et al., 2011) or XDS (Kabsch, 2010). The program Aimless was then used to scale the data sets (Evans, 2006). Inhibitor bound structures were refined using either PHENIX (Adams et al., 2009) and Refmac (Vagin et al., 2004) with inhibitor restraints built using PRODRG (Schuttelkopf and van Aalten, 2004).

Imidazole Displacement

Purified bsNOS was diluted to 2 μM into a buffered solution containing 50 mM Tris (pH 7.6), 10 mM NaCl, 100 μM dithiothreitol, and 1 mM imidazole to generate a low spin heme. NOS inhibitors were titrated into the bsNOS-buffered solution, and the conversion of the heme group from low spin to high spin was monitored using a Cary 3E UV-visible spectrophotometer. The K_S was calculated as previously described from the $K_{S,app}$ (Holden et al., 2013; Roman et al., 1995) using the bsNOS K_D imidazole at 384 μM and the bsNOS-I218V K_D imidazole at 506 μM (Wang et al., 2004).

Effect of Antimicrobial Induced Stress and NOS Inhibitors on S. aureus

Creation of the *S. aureus* UAMS1182 *nos* isogenic knockout is described in a previous report (van Sorge et al., 2013). Parent (wild type, *wt*) and knockout (Δ*nos*) were cultured in cation-adjusted Mueller Hinton broth (CAMHB). Prior to H_2O_2 assays, strains were cultured overnight at 37 °C then subcultured at a 1/20 dilution in fresh CAMHB. Strains were grown to mid-log phase (OD_{600} ~0.4), pelleted by centrifugation, washed twice in CAMHB, and diluted in CAMHB to a predetermined concentration approximating 2×10^7 colony forming units per mL (CFU/mL). Volumes of 25 μL (5×10^5 CFU) were dispensed to 96 well plates (Corning Life Sciences) in 200 μL aliquots of CAMHB and CAMHB with amendments including 5 mM H_2O_2 (Sigma), 200 μM **19**, 200 μM **32**, and equivalent control volumes of **19/32** solvent. Plates were incubated at 37 °C with shaking. Cultures were sampled at 30 min intervals by removing 25 μL for serial dilution in CAMHB and spot plating on Todd Hewitt agar (Becton Dickinson). Plates were incubated overnight and culture CFU/mL was calculated by enumerating counted colonies and multiplying back through the dilution factor. All conditions were sampled in triplicate; values presented are mean ± standard deviation. Statistical analysis was performed in Excel (Microsoft) using the Student's t-test.

NOS inhibitor cytotoxicity in mammalian cell culture

Cell toxicity assays were performed on mouse embryonic fibroblasts (MEF), which were maintained in DMEM (Corning Cell Gro, USA) media supplemented with 10% fetal calf serum (Sigma-Aldrich, USA) and 1% penicillin-streptomycin (Mediatech, Corning, USA) at ~70% confluency. Cell Titer Glo assays (Cell Titer Glo Luminescent Cell Viability Assay kit, Promega Corporation) were performed in a clear bottom 96-well black cell culture plates (Greiner Bio- One, NC, USA). After plating at 250 cells/well in a volume of 100 μl, cells were left undisturbed for at least 24 h before NOS inhibitor addition. NOS inhibitors **19, 32**, and L-NAME (Enzo Life Sciences) were added to the MEF's at 40 μM, 20 μM, 10 μM, 5 μM, 2.5 μM, 1.25 μM, 0.625 μM and 0.3125 μM. Cells were prepared for analysis 72 h after NOS inhibitors were added by addition of 10 μl of 0.1% Triton-X100 in PBS with shaking for 1 min at room temperature (RT). Cell Titer-Glo lysis reagent (20 μl) was then added followed by 1 min of shaking and a 10 min incubation in the dark at RT. Luminescence was detected using an IVIS imaging system (IVIS Lumina II, Perkin Elmer, USA). IC_{50} values were determined using the GraphPad Prism software (GraphPad Software, Inc, La Jolla, CA).

Chemical library preparation

Since bacterial NOS-selective inhibitors had not yet been identified, we collected a diverse set of NOS inhibitors (**1–25**) from our previous NOS studies (Holden et al., 2013; Huang et al., 2012; Huang et al., 2014; Jing et al., 2014; Kang et al., 2014; Kohanski et al., 2007) as well as several newly synthesized molecules (**26–36**). The collected small molecule library (**1–36**) was composed of a chemically diverse set of aminopyridine derivatives (aminopyridinyl-2-ethyl, aminopyridinyl-2-benzyl, aminopyridinyl-2-phenyl), 7-azaindoles, thiopheneamidines, and 2-aminoquinolines. In general, inhibitors **26–36** generally have arylalkyl side chains or a N^1,N^2-dimethylethane-1,2-diamine tail. Chemical syntheses and spectral validation of the NOS inhibitors are included in the Supplemental Information.

Chemical Synthesis

Details of the synthesis are provided in the Supplemental Material.

Supplementary Material

Refer to Web version on PubMed Central for supplementary material.

Acknowledgment

This work was supported by National Institutes of Health grants GM57353 (TLP), GM49725 (RBS), HD071600 (VN), and AI057153 (VN). We also thank the beamline staff at SSRL and ALS for their assistance during the remote X-ray diffraction data collections.

References

Adak S, Aulak KS, Stuehr DJ. Direct evidence for nitric oxide production by a nitric-oxide synthase-like protein from *Bacillus subtilis*. J Biol Chem. 2002; 277:16167–16171. [PubMed: 11856757]

Adams PD, Mustyakimov M, Afonine PV, Langan P. Generalized X-ray and neutron crystallographic analysis: more accurate and complete structures for biological macromolecules. Acta Crystallogr D Biol Crystallogr. 2009; 65:567–573. [PubMed: 19465771]

Battye TG, Kontogiannis L, Johnson O, Powell HR, Leslie AG. iMOSFLM: a new graphical interface for diffraction-image processing with MOSFLM. Acta Crystallogr D Biol Crystallogr. 2011; 67:271–281. [PubMed: 21460445]

Bird LE, Ren J, Zhang J, Foxwell N, Hawkins AR, Charles IG, Stammers DK. Crystal structure of SANOS, a bacterial nitric oxide synthase oxygenase protein from Staphylococcus aureus. Structure. 2002; 10:1687–1696. [PubMed: 12467576]

Chartier FJ, Couture M. Stability of the heme environment of the nitric oxide synthase from Staphylococcus aureus in the absence of pterin cofactor. Biophys J. 2004; 87:1939–1950. [PubMed: 15345570]

Cheng Y, Prusoff WH. Relationship between the inhibition constant (KI) and the concentration of inhibitor which causes 50 per cent inhibition (I50) of an enzymatic reaction. Biochem Pharmacol. 1973; 22:3099–3108. [PubMed: 4202581]

Cinelli MA, Li H, Chreifi G, Martasek P, Roman LJ, Poulos TL, Silverman RB. Simplified 2-aminoquinoline-based scaffold for potent and selective neuronal nitric oxide synthase inhibition. J Med Chem. 2014; 57:1513–1530. [PubMed: 24472039]

Delker SL, Xue F, Li H, Jamal J, Silverman RB, Poulos TL. Role of zinc in isoformselective inhibitor binding to neuronal nitric oxide synthase. Biochemistry. 2010; 49:10803–10810. [PubMed: 21138269]

Diekema DJ, Pfaller MA, Schmitz FJ, Smayevsky J, Bell J, Jones RN, Beach M, Group SP. Survey of infections due to Staphylococcus species: frequency of occurrence and antimicrobial susceptibility of isolates collected in the United States, Canada, Latin America, Europe, and the Western Pacific region for the SENTRY Antimicrobial Surveillance Program, 1997–1999. Clin Infect Dis. 2001; 32(Suppl 2):S114–S132. [PubMed: 11320452]

Evans P. Scaling and assessment of data quality. Acta Crystallogr D Biol Crystallogr. 2006; 62:72–82. [PubMed: 16369096]

Gardete S, Tomasz A. Mechanisms of vancomycin resistance in Staphylococcus aureus. J Clin Invest. 2014; 124:2836–2840. [PubMed: 24983424]

Gusarov I, Nudler E. NO-mediated cytoprotection: Instant adaptation to oxidative stress in bacteria. Proc Natl Acad Sci USA. 2005; 102:13855–13860. [PubMed: 16172391]

Gusarov I, Shatalin K, Starodubtseva M, Nudler E. Endogenous nitric oxide protects bacteria against a wide spectrum of antibiotics. Science. 2009; 325:1380–1384. [PubMed: 19745150]

Hannibal L, Somasundaram R, Tejero J, Wilson A, Stuehr DJ. Influence of hemethiolate in shaping the catalytic properties of a bacterial nitric-oxide synthase. J Biol Chem. 2011; 286:39224–39235. [PubMed: 21921039]

Hevel JM, White KA, Marletta MA. Purification of the inducible murine macrophage nitric oxide synthase. Identification as a flavoprotein. J Biol Chem. 1991; 266:22789–22791. [PubMed: 1720773]

Holden JK, Kang S, Hollingsworth SA, Li H, Lim N, Chen S, Huang H, Xue F, Tang W, Silverman RB, et al. Structure-based design of bacterial nitric oxide synthase inhibitors. J Med Chem. 2015; 58:994–1004. [PubMed: 25522110]

Holden JK, Li H, Jing Q, Kang S, Richo J, Silverman RB, Poulos TL. Structural and biological studies on bacterial nitric oxide synthase inhibitors. Proc Natl Acad Sci USA. 2013; 110:18127–18131. [PubMed: 24145412]

Holden JK, Lim N, Poulos TL. Identification of Redox Partners and Development of a Novel Chimeric Bacterial Nitric Oxide Synthase for Structure Activity Analyses. J Biol Chem. 2014; 289:29437–29445. [PubMed: 25194416]

Huang H, Ji H, Li H, Jing Q, Labby KJ, Martasek P, Roman LJ, Poulos TL, Silverman RB. Selective monocationic inhibitors of neuronal nitric oxide synthase. Binding mode insights from molecular dynamics simulations. J Am Chem Soc. 2012; 134:11559–11572. [PubMed: 22731813]

Huang H, Li H, Martasek P, Roman LJ, Poulos TL, Silverman RB. Structure-guided design of selective inhibitors of neuronal nitric oxide synthase. J Med Chem. 2013; 56:3024–3032. [PubMed: 23451760]

Huang H, Li H, Yang S, Chreifi G, Martasek P, Roman LJ, Meyskens FL, Poulos TL, Silverman RB. Potent and selective double-headed thiophene-2-carboximidamide inhibitors of neuronal nitric oxide synthase for the treatment of melanoma. J Med Chem. 2014; 57:686–700. [PubMed: 24447275]

Jevons MP, Rolinson GN, Knox R. Celbenin-Resistant Staphylococci. Brit Med J. 1961; 1:124-&.

Jing Q, Li H, Roman LJ, Martasek P, Poulos TL, Silverman RB. Combination of chiral linkers with thiophenecarboximidamide heads to improve the selectivity of inhibitors of neuronal nitric oxide synthase. Bioorg Med Chem Lett. 2014; 24:4504–4510. [PubMed: 25149509]

Kabsch W. Xds. Acta Crystallogr D Biol Crystallogr. 2010; 66:125–132. [PubMed: 20124692]

Kang S, Tang W, Li H, Chreifi G, Martasek P, Roman LJ, Poulos TL, Silverman RB. Nitric oxide synthase inhibitors that interact with both heme propionate and tetrahydrobiopterin show high isoform selectivity. J Med Chem. 2014; 57:4382–4396. [PubMed: 24758147]

Kohanski MA, Dwyer DJ, Hayete B, Lawrence CA, Collins JJ. A common mechanism of cellular death induced by bactericidal antibiotics. Cell. 2007; 130:797–810. [PubMed: 17803904]

Li H, Jamal J, Delker S, Plaza C, Ji H, Jing Q, Huang H, Kang S, Silverman RB, Poulos TL. The mobility of a conserved tyrosine residue controls isoform-dependent enzyme-inhibitor interactions in nitric oxide synthases. Biochemistry. 2014; 53:5272–5279. [PubMed: 25089924]

Loomba PS, Taneja J, Mishra B. Methicillin and Vancomycin Resistant S. aureus in Hospitalized Patients. J Glob Infect Dis. 2010; 2:275–283. [PubMed: 20927290]

Martasek P, Miller RT, Roman LJ, Shea T, Masters BS. Assay of isoforms of *Escherichia coli*-expressed nitric oxide synthase. Methods Enzymol. 1999; 301:70–78. [PubMed: 9919555]

Pant K, Bilwes AM, Adak S, Stuehr DJ, Crane BR. Structure of a nitric oxide synthase heme protein from *Bacillus subtilis* . Biochemistry. 2002; 41:11071–11079. [PubMed: 12220171]

Reece SY, Woodward JJ, Marletta MA. Synthesis of nitric oxide by the NOS-like protein from deinococcus radiodurans: a direct role for tetrahydrofolate. Biochemistry. 2009; 48:5483–5491. [PubMed: 19388666]

Roman LJ, Sheta EA, Martasek P, Gross SS, Liu Q, Masters BS. High-level expression of functional rat neuronal nitric oxide synthase in *Escherichia coli*. Proc Natl Acad Sci USA. 1995; 92:8428–8432. [PubMed: 7545302]

Schuttelkopf AW, van Aalten DM. PRODRG: a tool for high-throughput crystallography of protein-ligand complexes. Acta Crystallogr D Biol Crystallogr. 2004; 60:1355–1363. [PubMed: 15272157]

Shatalin K, Gusarov I, Avetissova E, Shatalina Y, McQuade LE, Lippard SJ, Nudler E. Bacillus anthracis-derived nitric oxide is essential for pathogen virulence and survival in macrophages. Proc Natl Acad Sci USA. 2008; 105:1009–1013. [PubMed: 18215992]

Silverman RB. Design of selective neuronal nitric oxide synthase inhibitors for the prevention and treatment of neurodegenerative diseases. Acc Chem Res. 2009; 42:439–451. [PubMed: 19154146]

Stefani S, Chung DR, Lindsay JA, Friedrich AW, Kearns AM, Westh H, Mackenzie FM. Meticillin-resistant Staphylococcus aureus (MRSA): global epidemiology and harmonisation of typing methods. Int J Antimicrob Agents. 2012; 39:273–282. [PubMed: 22230333]

Talbot GH, Bradley J, Edwards JE Jr, Gilbert D, Scheld M, Bartlett JG. Antimicrobial Availability Task Force of the Infectious Diseases Society of, A. Bad bugs need drugs: an update on the development pipeline from the Antimicrobial Availability Task Force of the Infectious Diseases Society of America. Clin Infect Dis. 2006; 42:657–668. [PubMed: 16447111]

Vagin AA, Steiner RA, Lebedev AA, Potterton L, McNicholas S, Long F, Murshudov GN. REFMAC5 dictionary: organization of prior chemical knowledge and guidelines for its use. Acta Crystallogr D Biol Crystallogr. 2004; 60:2184–2195. [PubMed: 15572771]

van Sorge NM, Beasley FC, Gusarov I, Gonzalez DJ, von Kockritz-Blickwede M, Anik S, Borkowski AW, Dorrestein PC, Nudler E, Nizet V. Methicillin-resistant *Staphylococcus aureus* bacterial nitric-oxide synthase affects antibiotic sensitivity and skin abscess development. J Biol Chem. 2013; 288:6417–6426. [PubMed: 23322784]

Wang ZQ, Wei CC, Sharma M, Pant K, Crane BR, Stuehr DJ. A conserved Val to Ile switch near the heme pocket of animal and bacterial nitric-oxide synthases helps determine their distinct catalytic profiles. J Biol Chem. 2004; 279:19018–19025. [PubMed: 14976216]

Yamamoto K, Shimamura K, Sekiguchi F, Sunano S. Effects of NG-nitro-L-arginine on the blood pressure of spontaneously hypertensive rats with different degrees of hypertension. Clin Exp Hypertens. 2001; 23:533–544. [PubMed: 11710755]

Yuste JE, Echeverry MB, Ros-Bernal F, Gomez A, Ros CM, Campuzano CM, Fernandez- Villalba E, Herrero MT. 7-Nitroindazole down-regulates dopamine/DARPP-32 signaling in neostriatal neurons in a rat model of Parkinson's disease. Neuropharmacology. 2012; 63:1258–1267. [PubMed: 22877786]

Highlights

- Inhibitors selective toward bacterial nitric oxide synthase have been identified.
- These inhibitors are antimicrobial against MRSA.
- Crystallography reveals the structural basis for selectivity.
- NOS inhibitor library to identify molecules with antimicrobial function.

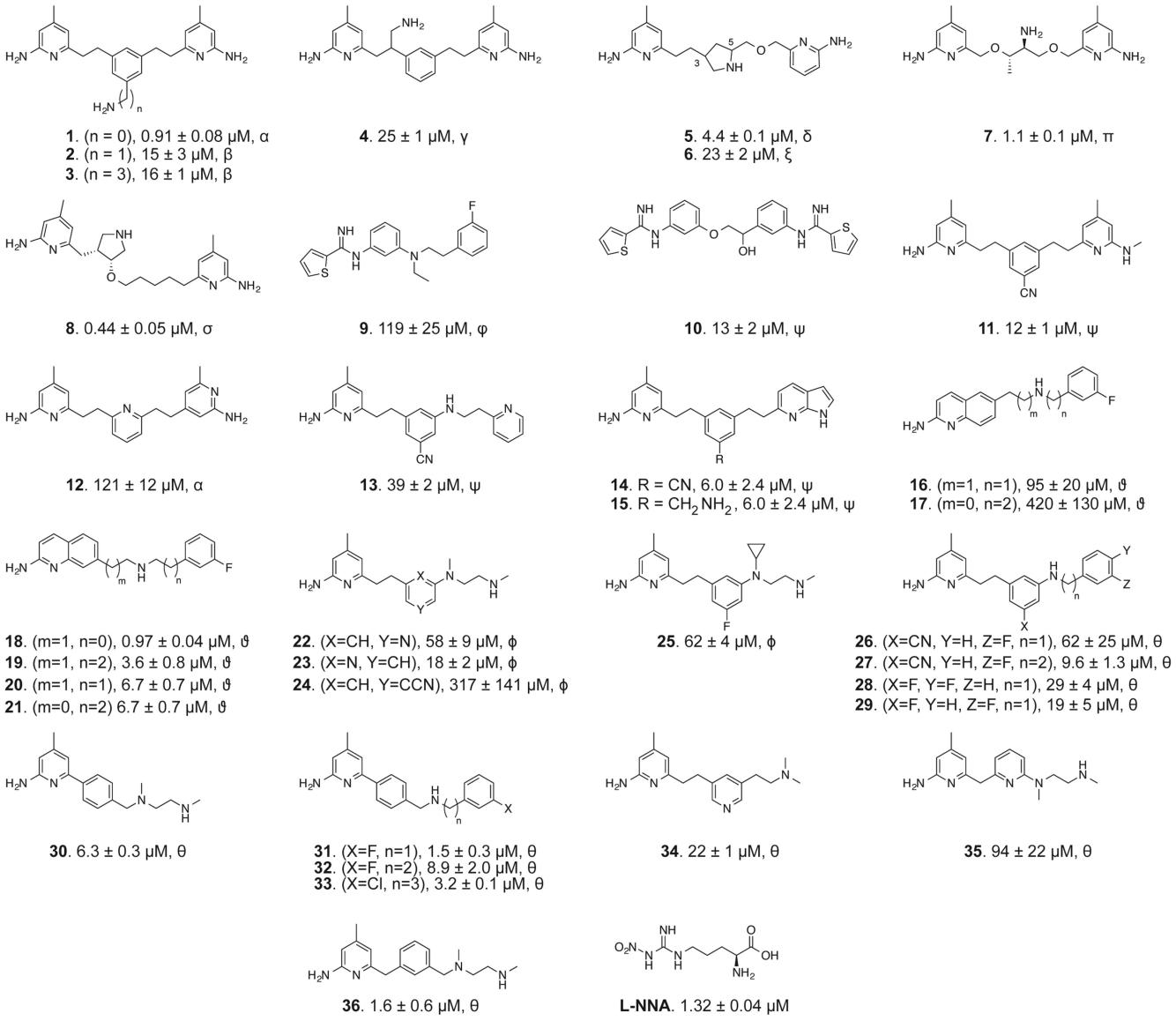

Figure 1.

NOS inhibitor library used in this study. The inhibitor K_S values, determined from an imidazole displacement assay are reported in μM for each inhibitor of bsNOS. Isolation and characterization of NOS inhibitors marked by α were previously reported in (Delker et al., 2010), β in (Huang et al., 2013), γ in (Huang et al., 2014), δ in (Holden et al., 2013), ξ in (Jing et al., 2014), π in (Holden et al., 2013), σ in (Huang et al., 2012), φ in (Huang et al., 2014), ψ (Holden et al., 2014), ϑ in (Cinelli et al., 2014), φ in (Kang et al., 2015, unpublished data), and θ reported here.

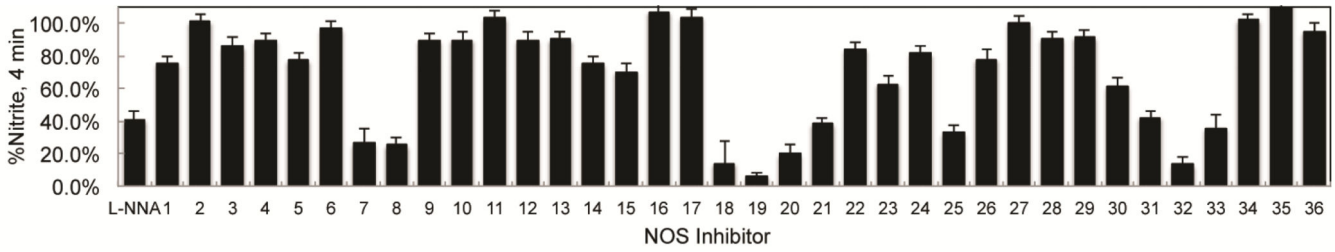

Figure 2.

On the basis of a single time point analysis using the bBiDomain for bacterial NOS inhibition, NOS inhibitors have varying potency toward bacterial NOS. Nitrite concentrations were measured after a 4 min incubation. Error bars represent the average ± the SEM for three separate experiments.

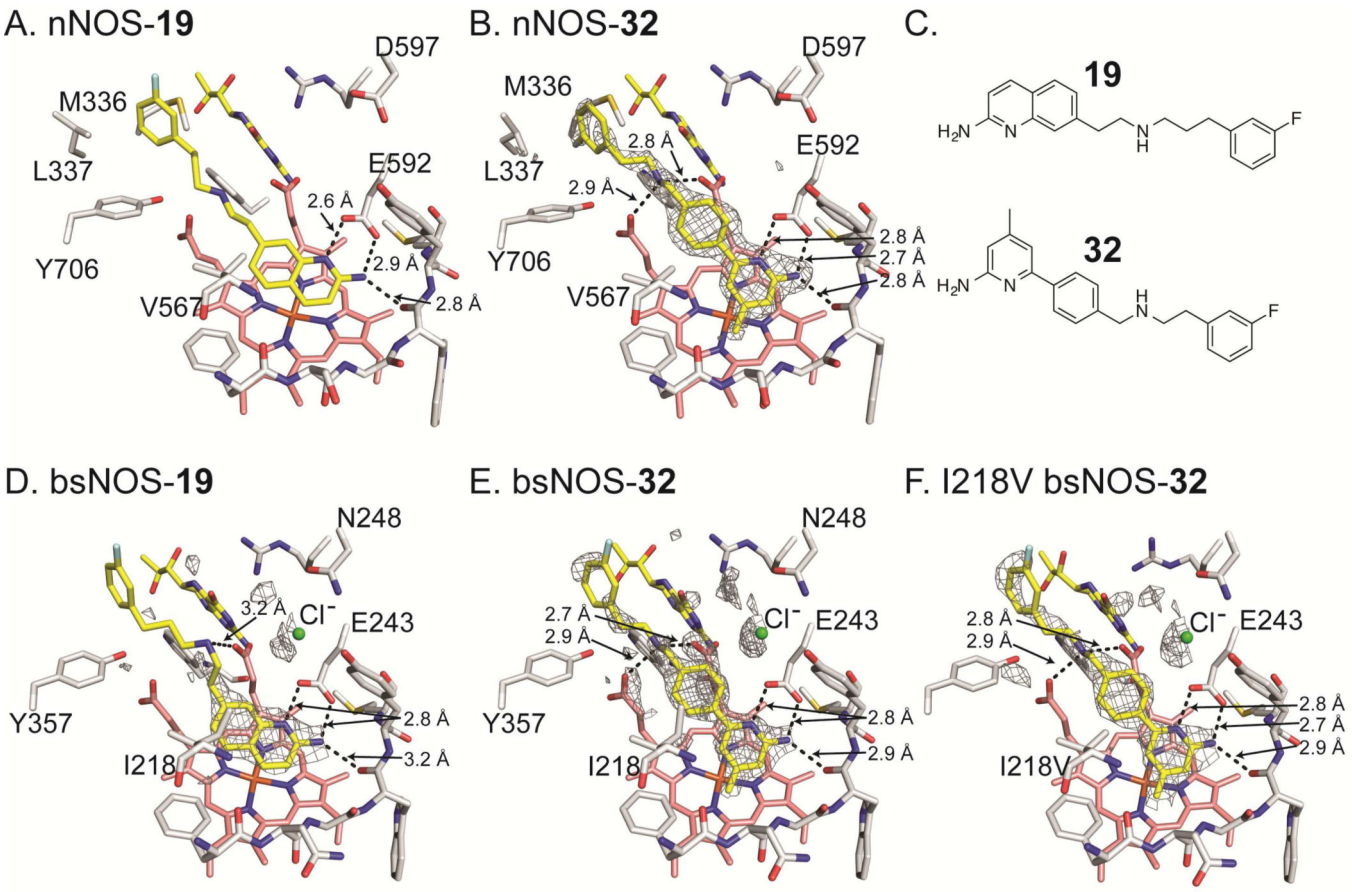

Figure 3.

Inhibitor bound NOS crystal structures with select side chains colored white, heme group colored salmon, and both the active site inhibitor and H_4B molecule colored yellow. For bsNOS inhibitor bound structures there is a chlorine ion bound at the carboxylate-binding site of L-Arg, which is shown as a green sphere. Both **19** and **32** bind to nNOS and bsNOS. In the nNOS structures (A and B) the fluorinated-benzyl group binds to a hydrophobic patch that is not present in bsNOS, adjacent to the heme propionate and composed of Y706, L337 and M336. At the NOS active sites both **19** and **32** bind in similar orientations to form a network of H bonds indicated by dashed lines. For the bsNOS structures, both **19** and **32** are within a hydrophobic contact of bsNOS I218. A) **19** bound to nNOS (PDB 4CAO). B) **32** bound to nNOS with the F_O-F_C map contoured at 4.0σ. C) Chemical representations of **19** and **32**. D) **19** bound to bsNOS with the F_O-F_C map contoured at 3.0σ. E) **32** bound to bsNOS with the F_O-F_C map contoured at 3.0σ. F) **32** bound to I218V bsNOS with the F_O-F_C map contoured at 3.0σ.

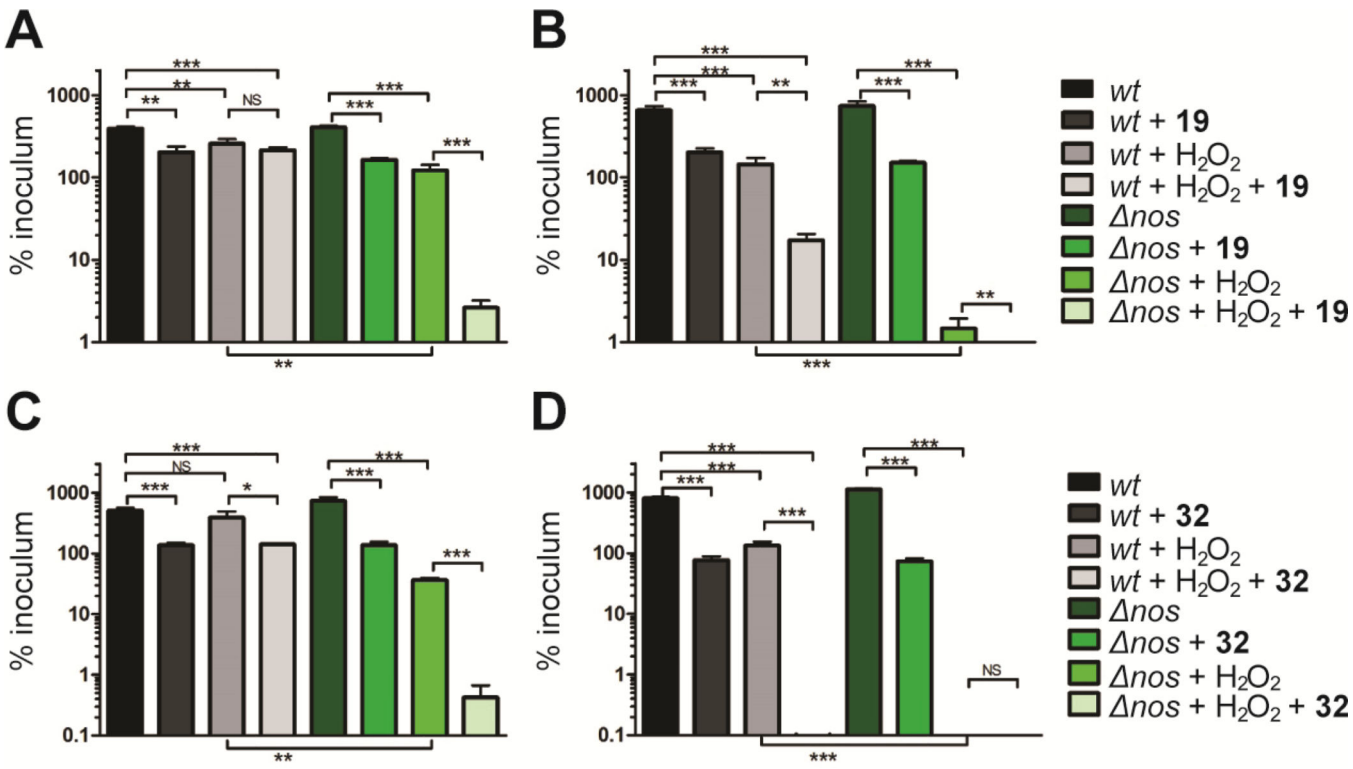

Figure 4.

NOS inhibitors and peroxide work synergistically to eliminate *S. aureus* over time. Colonies of *S. aureus* observed after A) 30 min and B) 60 min exposure to 200 μM **19** and/or 5 mM H_2O_2. Similarly, *S. aureus* viability was also measured at C) 30 min and D) 60 min following exposure to 200 μM **32** and/or 5 mM H_2O_2. Error bars represent the mean ± SD of 3 replicates. Students *t* test gives ***P < 0.001, **P < 0.01 and *P < 0.05.

Table 1

Inhibition of NOS isoforms by inhibitors **32** and **19**. The bBiDomain construct was used to evaluate inhibitor K_i against bsNOS.

Inhibitor	K_i bBiDomain (nM)	K_i nNOS (nM)	K_i iNOS (nM)	K_i eNOS (nM)
19	269	164	31900	7250
32	1940	525	6440	2870

Table 2

Data collection, processing and refinement statistics of the NOS inhibitor bound structures

PDB Code	bsNOS-19 4D7H	bsNOS-32 4D7J	bsNOS-32 4D7I
Data Collection			
Wavelength (Å)	0.976484	0.918370	0.999746
Space group	P21212	P21212	P21212
No. unique reflections	32128 (2261)	70341 (3408)	48394 (2575)
Cell dimensions			
a, *b*, *c* (Å)	80.9 94.7 62.8	80.5 94.8 62.8	80.6 95.0 61.6
α, β, γ (°)	90 90 90	90 90 90	90 90 90
Resolution (Å)	49.62 - 2.02 (2.07 - 2.02)	37.06 - 1.55 (1.58 - 1.55)	48.94 - 1.96 (2.01 - 1.96)
R_{merge}	0.128 (0.570)	0.052 (2.522)	0.135 (1.518)
R_{PIM}	0.078 (0.530)	0.033 (1.599)	0.096 (1.074)
$CC_{1/2}$	0.997 (0.834)	1.000 (0.528)	0.992 (0.558)
$I / \sigma I$	10.1 (1.6)	18.0 (0.6)	7.3 (1.0)
Completeness (%)	99.5 (97.5)	99.8 (99.8)	99.6 (100.0)
Redundancy	5.2 (3.0)	6.5 (6.7)	4.3 (4.4)
Refinement			
Resolution (Å)	49.62 - 2.02 (2.092 - 2.02)	37.061 - 1.550 (1.605 - 1.55)	48.94 - 1.96 (2.03 - 1.96)
No. reflections used	31936	70050	34419
Completeness (%)	98.8	99.45	99.23
R_{work}	0.1849 (0.2734)	0.173 (0.3612)	0.1893 (0.3501)
R_{free}	0.2377 (0.3350)	0.2035 (0.3715)	0.2352 (0.3622)
No. of atoms	3257	3468	3253
macromolecules	2952	2950	2940
ligands	101	121	92
solvent	204	397	221
Average B-factor	41.4	28.7	41.1
macromolecules	41.4	27.7	41.2
ligands	42.8	29.5	34.5
solvent	41.9	36.4	42.9
R.m.s deviations			
Bond lengths (Å)	0.007	0.007	0.008
Bond angles (°)	1.177	1.195	1.19

* Values in parentheses are for highest-resolution shell.

Table 3

Calculated K_S values by imidazole displacement for NOS ligands to bsNOS.

Ligand	WT -K_S (μM)	I218V - K_S (μM)
L-Arg	4.8 ± 0.1 (Wang et al., 2004)	2.0 ± 0.2 (Wang et al., 2004)
19	3.6 ± 0.8	18 ± 2
32	8.9 ± 2.0	58 ± 4